

# A statistical interpretation of the correlation between intermediate mass fragment multiplicity and transverse energy

L. Phair<sup>1</sup>, L. Beaulieu<sup>1,\*</sup>, L.G. Moretto<sup>1</sup>, G.J. Wozniak<sup>1</sup>, D. R. Bowman<sup>2,†</sup>, N. Carlin<sup>2,§</sup>, L. Celano<sup>5</sup>, N. Colonna<sup>5</sup>, J.D. Dinius<sup>2</sup>, A. Ferrero<sup>3</sup>, C.K. Gelbke<sup>2</sup>, T. Glasmacher<sup>2</sup>, F. Gramegna<sup>6</sup>, D.O. Handzy<sup>2</sup>, W.C. Hsi<sup>2</sup>, M.J. Huang<sup>2</sup>, I. Iori<sup>3</sup>, Y.D. Kim<sup>2,||</sup>, M.A. Lisa<sup>2,¶</sup>, W.G. Lynch<sup>2</sup>, G.V. Margagliotti<sup>4</sup>, P.F. Mastinu<sup>7,\*\*</sup>, P.M. Milazzo<sup>7,\*\*</sup>, C.P. Montoya<sup>2</sup>, A. Moroni<sup>3</sup>, G.F. Peaslee<sup>2,††</sup>, R. Rui<sup>4</sup>, C. Schwarz<sup>2</sup>, M.B. Tsang<sup>2</sup>, K. Tso<sup>1</sup>, G. Vannini<sup>4</sup>, F. Zhu<sup>2</sup>

<sup>1</sup>*Nuclear Science Division, Lawrence Berkeley National Laboratory, Berkeley, California 94720*

<sup>2</sup>*National Superconducting Cyclotron Laboratory and Department of Physics and Astronomy, Michigan State University, East Lansing, MI 48824*

<sup>3</sup>*Istituto Nazionale di Fisica Nucleare and Dipartimento di Fisica, Via Celoria 16, 20133 Milano, Italy*

<sup>4</sup>*Dipartimento di Fisica and Istituto Nazionale di Fisica Nucleare, Via A. Valerio 2, 34127 Trieste, Italy*

<sup>5</sup>*Istituto Nazionale di Fisica Nucleare, Via Amendola 173, 70126 Bari, Italy*

<sup>6</sup>*Istituto Nazionale di Fisica Nucleare, Laboratori Nazionali di Legnaro, Via Romea 4, 35020 Legnaro, Italy*

<sup>7</sup>*Dipartimento di Fisica and Istituto Nazionale di Fisica Nucleare, Bologna, Italy*

(December 2, 2017)

Multifragment emission following  $^{129}\text{Xe}+^{197}\text{Au}$  collisions at 30, 40, 50 and 60 AMeV has been studied with multidetector systems covering nearly  $4\pi$  in solid angle. The correlations of both the intermediate mass fragment and light charged particle multiplicities with the transverse energy are explored. A comparison is made with results from a similar system,  $^{136}\text{Xe}+^{209}\text{Bi}$  at 28 AMeV. The experimental trends are compared to statistical model predictions.

## I. INTRODUCTION

Nuclear multifragmentation is arguably the most complex nuclear reaction, involving both collective and internal degrees of freedom to an extent unmatched even by fission. As in fission, multifragmentation is expected to present a mix of statistical and dynamical features.

A substantial body of evidence has been presented in favor of the statistical nature of several features such as fragment multiplicities [1–10], charge distributions [11,12], and angular distributions [13]. Recently however, evidence has been put forth for the lack of statistical competition between intermediate mass fragment (IMF) emission and light charged particle (LCP) emission. More specifically, it has been shown that for the reaction  $^{136}\text{Xe}+^{209}\text{Bi}$  at 28 AMeV: a) LCP emission saturates with increasing number of emitted IMFs [14]; b) with increasing transverse energy ( $E_t$ ), the contribution of the LCPs to  $E_t$  saturates while that of the IMFs becomes dominant [15]; c) there is a strong anti-correlation of the leading fragment kinetic energy with the number of IMFs emitted [14]. This body of evidence seems to suggest that beyond a certain amount of energy deposition most, if not all, of the energy goes into IMF production rather than into LCP emission in a manner inconsistent with statistical competition.

Given the importance of these results in showing a potential failure of the statistical picture and a possible novel dynamical mechanism of IMF production, we have applied the same analysis to a set of systematic measurements of  $^{129}\text{Xe}+^{197}\text{Au}$  at several bombarding energies. In what follows we report on 1) new experimental data that confirm the general nature of the observations in [14]; 2) new experimental data which show trends that are different from those observed in [15]; 3) the effectiveness of gating on IMF multiplicity ( $N_{\text{IMF}}$ ) as an event-selection strategy; and 4) the reproduction of key results with statistical model calculations.

## II. EXPERIMENTAL SETUP

LCP and IMF yields and their correlations with, and contributions to  $E_t$  were determined for the reaction  $^{129}\text{Xe}+^{197}\text{Au}$  at 30, 40, 50, and 60 AMeV. The experiments were performed at the National Superconducting Cyclotron Laboratory at Michigan State University (MSU). Beams of  $^{129}\text{Xe}$ , at intensities of about  $10^7$  particles per second, irradiated gold targets of approximately  $1\text{ mg/cm}^2$ . The beam was delivered to the 92 inch scattering chamber with a typical beam spot diameter of 2-3 mm.

For the bombarding energies of 40, 50 and 60 AMeV, LCPs and IMFs emitted at laboratory angles of  $16^\circ$ – $160^\circ$  were detected using the MSU Miniball [16]. As configured for this experiment, the Miniball consisted of 171 fast plastic ( $40\text{ }\mu\text{m}$ )-CsI(2 cm) phoswich detectors, with a solid angle coverage of approximately 87% of  $4\pi$ . Identification thresholds for  $Z=3,10$ , and 18 fragments were  $\approx 2, 3$ , and 4 MeV/nucleon, respectively. Less energetic charged particles with energies greater than 1 MeV/nucleon were detected in the fast plastic scintillator foils, but were not identified by  $Z$  value. Isotopic identification was achieved for hydrogen and helium isotopes

with energies less than 75 MeV/nucleon. Energy calibrations were performed using elastically scattered  $^{12}\text{C}$  beams at forward angles and by using the punch-through points of the more backward detectors to normalize to existing data [17]. The energy calibrations are estimated to be accurate to about 10% at angles less than  $31^\circ$  and to about 20% for the more backward angles.

Particles going forward ( $\leq 16^\circ$ ) were measured with the LBL forward array [18], a high resolution Si-Si(Li)-plastic scintillator array. Fragments of charge  $Z=1-54$  were detected with high resolution using a 16-element Si( $300\ \mu\text{m}$ )-Si(Li)(5 mm)-plastic(7.6 cm) array [18] with a geometrical efficiency of  $\approx 64\%$ . Where counting statistics allowed, individual atomic numbers were resolved for  $Z=1-54$ . Representative detection thresholds of  $Z=2, 8, 20$  and  $54$  fragments were approximately 6, 13, 21, and 27 MeV/nucleon, respectively. Energy calibrations were obtained by directing 18 different beams ranging from  $Z=1$  to 54 into each of the 16 detector elements. The energy calibration of each detector was accurate to better than 1%, and position resolutions of  $\pm 1.5$  mm were obtained.

The complete detector system for these higher energies (LBL array + Miniball) subtended angles from  $2^\circ-160^\circ$  and had a geometric acceptance  $\approx 88\%$  of  $4\pi$ . As a precaution against secondary electrons, detectors at angles larger than  $100^\circ$  were covered with Pb-Sn foils of thickness  $5.05\ \text{mg}/\text{cm}^2$  (this increased the detection thresholds for these backward detectors). Both the Miniball and forward array were cooled and temperature stabilized.

For the 30 AMeV data set, the forward going particles ( $\theta = 8^\circ - 23^\circ$ ) were measured by the MULTICS array [19], a high resolution gas-Si-Si(Li)-CsI array. Detection thresholds were approximately 2.5 MeV/nucleon for all fragments ( $Z=1-54$ ), and the resolution in  $Z$  was much better than 1 unit for  $Z < 30$ . Energy calibrations were performed by directing 18 separate beams into each of the 36 telescopes. The calibration beams had energies of  $E/A=30$  and 70 MeV, and ranged in mass from  $^{12}\text{C}$  to  $^{129}\text{Xe}$ . An energy resolution of better than 2% was obtained. Position calibrations of the Si elements of the MULTICS array were performed with the procedure of ref. [20]. The angular resolution was estimated to be  $\approx 0.2^\circ$ . Charged particles emitted beyond  $23^\circ$  were detected with the Miniball in a setup similar to the higher bombarding energies described above. The complete detector system covered approximately 87% of  $4\pi$ .

Data were taken under two trigger conditions: at least two Miniball elements triggered or at least one IMF observed in the relevant forward array.

Further details of the experimental setups can be found in refs. [21,22].

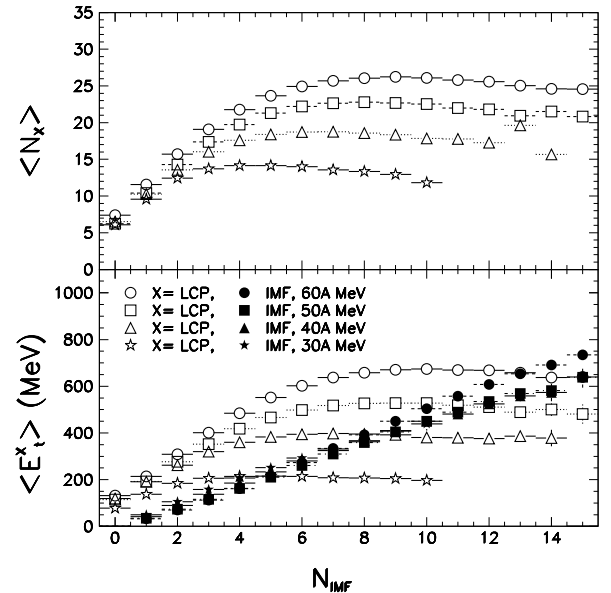


FIG. 1. The average LCP multiplicity (top panel), average transverse energy of IMFs (solid symbols), and average  $E_t$  of LCPs (open symbols, bottom panel) are plotted as a function of IMF multiplicity for the reaction  $^{129}\text{Xe}+^{197}\text{Au}$  at bombarding energies between 30 and 60 AMeV.

TABLE I. Values are given for the approximate  $N_{\text{IMF}}$  saturation value (along with the upper limit of the integrated cross section in percent), the average LCP multiplicity and average  $E_t^{\text{LCP}}$  in the saturation region of Fig. 1, and the maximum average IMF multiplicity for the top 5% of the  $E_t$  selected events, for the reaction  $^{129}\text{Xe}+^{197}\text{Au}$ .

$E_{\text{beam}}/A$	$N_{\text{IMF}}^{\text{sat}}$	$\langle N_{\text{LCP}} \rangle_{\text{max}}$	$\langle E_t^{\text{LCP}} \rangle_{\text{max}}$	$\langle N_{\text{IMF}} \rangle_{\text{max}}$
30 MeV	5 (6.5%)	13.9	220 MeV	4.6
40 MeV	7 (5.0%)	18.9	400 MeV	6.0
50 MeV	8 (4.3%)	23.1	530 MeV	6.9
60 MeV	8 (5.9%)	26.1	660 MeV	7.4

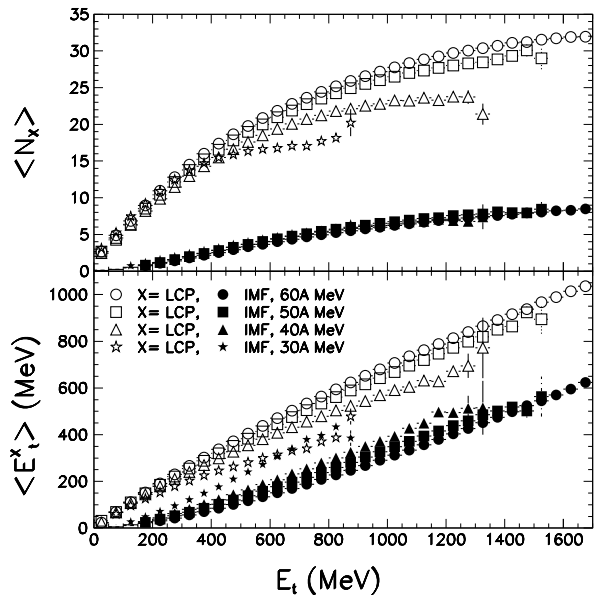


FIG. 2. The average IMF multiplicity (solid symbols, top panel), average LCP multiplicity (open symbols, top panel), average transverse energy of IMFs (solid symbols, bottom panel), and average transverse energy of LCPs (open symbols, bottom panel) are plotted as a function of  $E_t$ .

### III. COMPARISON WITH PREVIOUS RESULTS

Following the procedure outlined in [14], the average LCP yields were determined as a function of  $N_{\text{IMF}}$  (which serves as a rough measure of impact parameter or energy deposition). Fig. 1 shows an example of such an analysis for the reaction  $^{129}\text{Xe}+^{197}\text{Au}$  at bombarding energies between 30 and 60 AMeV. The average LCP multiplicity ( $\langle N_{\text{LCP}} \rangle$ ) does indeed saturate with increasing  $N_{\text{IMF}}$ , as observed in [14]. However, the value to which  $\langle N_{\text{LCP}} \rangle$  saturates ( $\langle N_{\text{LCP}} \rangle_{\text{max}}$ ) rises with increasing bombarding energy and is listed in Table I. The IMF multiplicity at which the saturation occurs is approximately 4-5 at 30 AMeV and rises with increasing bombarding energy to a value of 8-9 at 60 AMeV.

The average LCP contribution to  $E_t$  ( $\langle E_t^{\text{LCP}} \rangle$ ) saturates in a bombarding energy dependent fashion as well (see  $\langle E_t^{\text{LCP}} \rangle_{\text{max}}$  in Table I and open symbols of Fig. 1, bottom panel). In contrast, the average IMF contribution to  $E_t$  ( $\langle E_t^{\text{IMF}} \rangle$ ) rises linearly with increasing IMF multiplicity. The significance of the bombarding energy dependence of these observations will be discussed in the next section.

We now explore the dependence of these same variables on  $E_t$ . According to the procedure outlined in [15], the average yields of multiplicity and transverse energy for both IMFs and LCPs were determined as a function of  $E_t$  (which serves as a measure of impact parameter or energy deposition [23–25]). In Fig. 2 are plotted  $\langle N_{\text{IMF}} \rangle$ ,  $\langle N_{\text{LCP}} \rangle$ ,  $\langle E_t^{\text{IMF}} \rangle$ , and  $\langle E_t^{\text{LCP}} \rangle$  as a function of  $E_t$  for

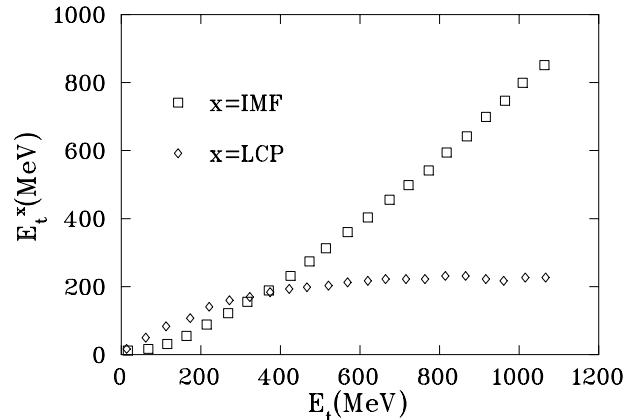


FIG. 3. The average transverse energies of IMFs (squares) and of LCPs (diamonds) are plotted as a function of  $E_t$  for the reaction  $^{136}\text{Xe}+^{209}\text{Bi}$  at 28 AMeV (taken from ref. [15]).

bombarding energies between 30 and 60 AMeV. All the observables rise with increasing  $E_t$ , in disagreement with the observations in [15]. In [15], the value of  $\langle E_t^{\text{LCP}} \rangle$  is observed to saturate to a relatively small value compared to  $\langle E_t^{\text{IMF}} \rangle$  (see Fig. 3), which is at variance with the observations in Fig. 2. The origin of this disagreement will be discussed in the next section.

Lastly, according to the procedure in [14], the average kinetic energy of the projectile-like fragment ( $\langle E/A \rangle_{\text{PLF}}$ , defined as the heaviest forward-moving particle in an event, with  $Z_{\text{PLF}} \geq 10$  and  $\theta \leq 23^\circ$ ) has been determined as a function of  $N_{\text{IMF}}$ , an example of which is given in Fig. 4. Here, we confirm the observation in [14]. For increasing  $N_{\text{IMF}}$ , the energy per nucleon of the leading fragment decreases continuously.

The three aforementioned observations have been used to suggest that, above a certain excitation energy, the IMFs get the lion's share of the energy while the LCPs lose their capability to compete [14,15]. In the following section, we explore each of these observations and suggest possible alternative explanations.

### IV. INTERPRETATION

We begin with the saturation of  $\langle N_{\text{LCP}} \rangle$  and  $\langle E_t^{\text{LCP}} \rangle$  as opposed to the continuous rise of  $\langle E_t^{\text{IMF}} \rangle$  observed in Fig. 1.  $\langle E_t^{\text{IMF}} \rangle$  rises linearly since

$$\langle E_t^{\text{IMF}} \rangle = \left\langle \sum_{i=1}^{N_{\text{IMF}}} E_i \sin^2 \theta_i \right\rangle \approx N_{\text{IMF}} \langle \epsilon_t^{\text{IMF}} \rangle, \quad (1)$$

where  $\langle \epsilon_t^{\text{IMF}} \rangle$  is the average transverse energy of an IMF. Thus, the reason for the continuous rise of  $\langle E_t^{\text{IMF}} \rangle$  can be understood quite simply. But what is the reason for the saturation of  $\langle E_t^{\text{LCP}} \rangle$  and  $\langle N_{\text{LCP}} \rangle$ ? We believe that the values of  $N_{\text{IMF}}$  where  $\langle N_{\text{LCP}} \rangle$  and  $\langle E_t^{\text{LCP}} \rangle$  saturate

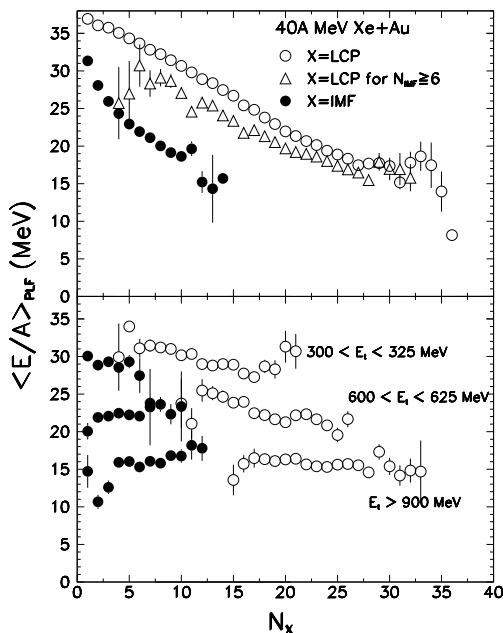


FIG. 4. Top panel: the average kinetic energy per nucleon of the projectile-like fragment is plotted as a function of  $N_{\text{IMF}}$  (solid circles) and  $N_{\text{LCP}}$  (open symbols). Bottom panel: Same as top panel but selected from events within the indicated range of  $E_t$ .

represent the tails of the IMF multiplicity distribution which are determined by the most central collisions.

For example, the values of IMF multiplicity at which the observables in Fig. 1 saturate ( $N_{\text{IMF}}^{\text{sat}}$ ) can be understood in terms of an impact parameter scale. Consider the probability  $P$  of emitting  $N_{\text{IMF}}$  and its integrated yield

$$S(N_{\text{IMF}}) = \sum_{i=N_{\text{IMF}}}^{\infty} P(i) \quad (2)$$

as shown in Fig. 5 for the reaction  $^{129}\text{Xe}+^{197}\text{Au}$  at 50 A MeV. Average impact parameter scales, as they are commonly employed, are proportional to  $\sqrt{S}$  [23]. Note that the multiplicities at which saturation occurs represent roughly 5% of the total integrated cross section (dashed line in the bottom panel of Fig. 5). The  $N_{\text{IMF}}$  value  $N_{\text{IMF}}^{\text{sat}}$  for which  $S \approx 0.05$  is listed in Table I for each of the different bombarding energies.  $N_{\text{IMF}}^{\text{sat}}$  tracks rather well the maximum average IMF multiplicity ( $\langle N_{\text{IMF}} \rangle_{\text{max}}$ ) measured for the most central collisions (top 5% of events) based upon the  $E_t$  scale.

The above observations demonstrate that large IMF multiplicities ( $N_{\text{IMF}} > \langle N_{\text{IMF}} \rangle_{\text{max}}$ ) have small probabilities and represent the extreme tails of events associated with the most central collisions. In other words, events with increasing values of  $N_{\text{IMF}}$  in the saturation region of Fig. 1 do not come from increasingly more central collisions where more energy has been dissipated. Thus,

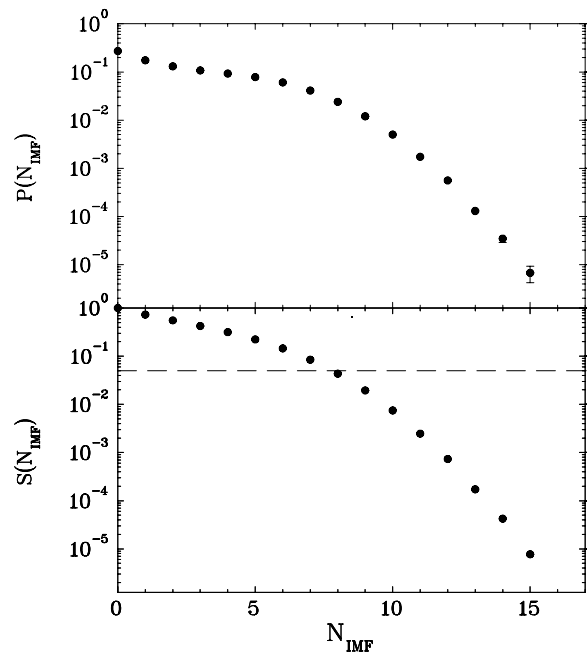


FIG. 5. Top panel: Probability to emit  $N_{\text{IMF}}$  from the reaction  $^{129}\text{Xe}+^{197}\text{Au}$  at 50 A MeV. Bottom panel: Integrated probability to emit  $N_{\text{IMF}}$  or more IMFs.

$N_{\text{IMF}}$  is useful as a global event selector over only a very limited range.

Consequently, it is expected that statistical models should exhibit similar trends as those observed in Fig. 1. Examples of such predictions are shown in Fig. 6 for the statistical multifragmentation model SMM (open symbols) [26] and for percolation (solid symbols) [27]. In both models an excitation energy ( $E$ ) distribution was used to mimic an impact parameter ( $b$ ) weighting. Assuming that  $b=0$  events give rise to the maximum excitation energy ( $E_{\text{max}}$ ), we have chosen the number of events at a given  $E$  proportional to  $E_{\text{max}} - E$ . The “excitation energy” for the percolation calculation is essentially represented by the number of broken bonds and is calculated as per ref. [27].

Both calculations show a saturation of  $\langle N_{\text{LCP}} \rangle$  when plotted as a function of IMF multiplicity. This behavior can be understood in terms of a simple model. Consider the statistical emission of two particle types with barriers  $B_1$  and  $B_2$  (and  $B_2 > B_1$ ). Assume the emission probabilities are  $p_i \propto \exp[-B_i/T]$  ( $i = 1, 2$ ) with  $p_1 + p_2 = 1$ . With the temperature  $T$  characterized in terms of the total multiplicity  $n_{\text{tot}} = n_1 + n_2 = \alpha T$ , and ignoring mass conservation, the solution for  $\langle n_1 \rangle$  as a function of  $n_2$  can be calculated for a distribution of excitation energies like that described above. The solution of this model is shown by the asterisk symbols in the top right panel of Fig. 6 for  $B_1=8$ ,  $B_2=24$ ,  $T_{\text{max}}=10$  and  $\alpha = 2$  (and  $N_{\text{IMF}}=n_2$ ,  $N_{\text{LCP}}=n_1$ ). This saturation is qualitatively similar to that of the other statistical models listed in Fig. 6 and to the behavior observed in Fig. 1. Furthermore, the satu-

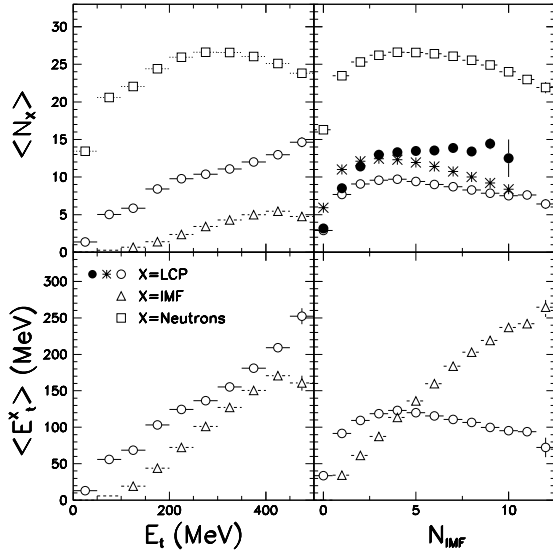


FIG. 6. Statistical model predictions from SMM (open symbols), percolation (solid symbols), and the simple model described in the text (crossed symbols). Upper left: the predicted average LCP and IMF multiplicities are plotted as a function of  $E_t$  for the decay of an ensemble of gold nuclei with excitation energies between 0.5-6.0 AMeV. Upper right: the average LCP and neutron multiplicities are plotted as a function of  $N_{IMF}$ . Lower left: the average  $E_t$  of the LCPs and IMFs as a function of  $E_t$  is shown. Lower right: the average  $E_t$  of the LCPs and IMFs is shown as a function of  $N_{IMF}$ .

ration value of  $\langle N_{LCP} \rangle$ , as well as the value of  $N_{IMF}$  at which saturation occurs, both depend on the maximum energy used in the calculation. Consequently, for statistical emission one expects (and observes in Fig. 1) a bombarding energy dependence of the saturation which reflects the total energy available to the decaying system. These behaviors are generic features that are present in any statistical model [28].

For completeness, the IMF and LCP yields from the SMM calculations are plotted as a function of  $E_t$  as well in Fig. 6 (left panels). There is no saturation of  $\langle E_t^{LCP} \rangle$  with increasing  $E_t$  as was observed in [15]. Instead, this calculation shows qualitatively the same trends as experimentally observed in Fig. 2.

What then causes the (unconfirmed) saturation of  $\langle E_t^{LCP} \rangle$  observed in  $^{136}\text{Xe}+^{209}\text{Bi}$  [15] (bottom panel of Fig. 7)? We believe that the saturation observed in  $^{136}\text{Xe}+^{209}\text{Bi}$  is likely due to the limited dynamic range of the detectors used. The charged particle yields from the  $^{136}\text{Xe}+^{209}\text{Bi}$  reaction were measured with the dwarf array [29] whose thin CsI crystals (thickness of 4 mm for polar angle  $\theta = 55 - 168^\circ$ , 8mm for  $\theta = 32 - 55^\circ$  and 20 mm for  $\theta = 4 - 32^\circ$ ) are unable to stop energetic LCPs. For example, protons punch through 4 mm of CsI at an energy of 30 MeV. Consequently, their contribution to  $E_t$  could be significantly underestimated.

An example of the distortions that would be caused by

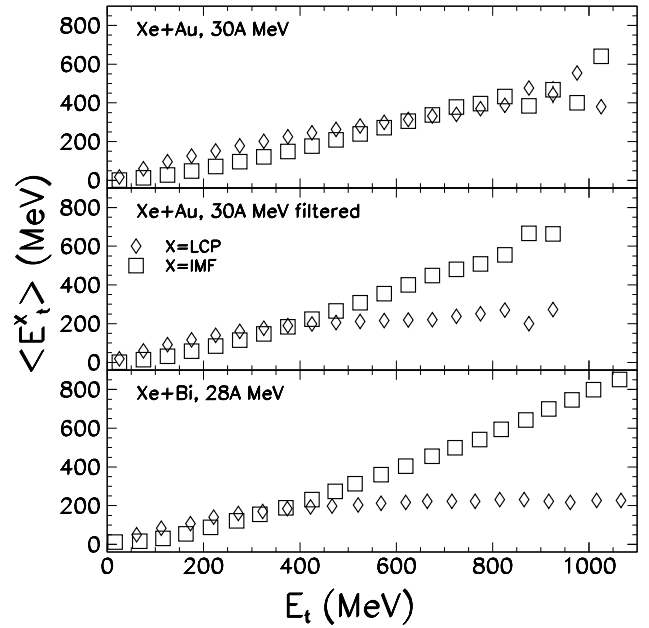


FIG. 7. The average transverse energies of IMFs (squares) and of LCPs (diamonds) are plotted as a function of  $E_t$  for the reactions  $^{129}\text{Xe}+^{197}\text{Au}$  at 30 AMeV (top panel),  $^{129}\text{Xe}+^{197}\text{Au}$  again but filtered with the upper energy thresholds of the dwarf array detector [29] (middle panel), and  $^{136}\text{Xe}+^{209}\text{Bi}$  at 28 AMeV (bottom panel, taken from ref. [15]).

the detector response of the dwarf array on the similar  $^{129}\text{Xe}+^{197}\text{Au}$  reaction at 30 AMeV is given in Fig. 7. In the top panel is plotted  $\langle E_t^{LCP} \rangle$  and  $\langle E_t^{IMF} \rangle$  as a function of  $E_t$  as measured by the MULTICS/Miniball collaboration. The thicknesses of the CsI crystals from these detectors range from 20 to 40 mm. Protons punch through 20 mm of CsI with an energy of 76 MeV. In the middle panel of Fig. 7, the  $^{129}\text{Xe}+^{197}\text{Au}$  data have been “filtered” using the dwarf array high energy cutoffs which remove high energy particles from  $E_t$ . After filtering, the two prominent features observed in the  $^{136}\text{Xe}+^{209}\text{Bi}$  data set [15] (bottom panel of Fig. 7) then appear in the filtered data. Namely,  $\langle E_t^{LCP} \rangle$  saturates to a small value and  $\langle E_t^{IMF} \rangle$  becomes the “apparent” dominant carrier of  $E_t$ . These two features are likely to be instrumental in origin and therefore do not warrant a physical interpretation.

Last of all, we come to the behavior of the average kinetic energy of the projectile-like fragment  $\langle E/A \rangle_{PLF}$  as a function of  $N_{IMF}$ , an example of which is given in Fig. 4 for  $^{129}\text{Xe}+^{197}\text{Au}$  at 40 AMeV (solid circles). From the decrease of  $\langle E/A \rangle_{PLF}$  with  $N_{IMF}$ , it was concluded that kinetic energy of the PLF is expended for the production of IMFs [14]. It was also argued that for increasing IMF multiplicity, the saturation of  $\langle N_{LCP} \rangle$  represents a critical excitation energy value beyond which no further amount of relative kinetic energy between the PLF and TLF is converted into heat. In other words, the IMFs no

longer compete with the LCPs for the available energy – they get it all.

One can test the consistency of this explanation by studying the same observable,  $\langle E/A \rangle_{\text{PLF}}$ , but now as a function of  $N_{\text{LCP}}$  (open symbols, top panel of Fig. 4). We observe the same dependence as that of the IMFs – a monotonic decrease of  $\langle E/A \rangle_{\text{PLF}}$  with increasing  $N_{\text{LCP}}$  which reaches a value of  $\approx 17$  MeV at the largest multiplicities. This behavior persists whether we restrict ourselves to the saturation region ( $N_{\text{IMF}} \geq 6$ , triangles) or not (open circles). The similar behavior of  $\langle E/A \rangle_{\text{PLF}}$  with respect to  $N_{\text{IMF}}$  and  $N_{\text{LCP}}$  indicates that the LCPs do compete with the IMFs for the available energy.

This can be seen more clearly by pre-selecting events with a better global observable,  $E_t$  [24,25,30], as done in the bottom panel of Fig. 4. Once a window of  $E_t$  is selected, a corresponding value of  $\langle E/A \rangle_{\text{PLF}}$  is also determined, and there is no longer any strong dependence of  $\langle E/A \rangle_{\text{PLF}}$  on  $N_{\text{IMF}}$  or  $N_{\text{LCP}}$ . In fact, the resulting  $N_{\text{IMF}}$  and  $N_{\text{LCP}}$  selections both give the *same* value of  $\langle E/A \rangle_{\text{PLF}}$ , consistent with a scenario where both species compete for the same available energy.

## V. CONCLUSIONS

In summary, we have made a systematic study of LCP and IMF observables as a function of IMF multiplicity and transverse energy for the reaction  $^{129}\text{Xe}+^{197}\text{Au}$  at bombarding energies between 30 and 60 AMeV.

We observe that  $\langle N_{\text{LCP}} \rangle$  and  $\langle E_t^{\text{LCP}} \rangle$  saturate as a function of  $N_{\text{IMF}}$  in a bombarding energy dependent way. These saturations are predicted by statistical models and are fundamental features of statistical decay [28]. A bombarding energy dependence of  $\langle N_{\text{LCP}} \rangle$ ,  $\langle E_t^{\text{LCP}} \rangle$ , and  $N_{\text{IMF}}^{\text{sat}}$  is expected (and experimentally observed) within the framework of statistical decay.

In addition, it has been demonstrated in a model independent fashion that the LCPs compete with the IMFs for the available energy. By using  $E_t$ , a more sensitive event selection is obtained. The analysis also demonstrates the limited usefulness of event classification using only  $N_{\text{IMF}}$ .

We do not observe a saturation of  $\langle E_t^{\text{LCP}} \rangle$  as a function of  $E_t$  at any bombarding energy. The saturation of  $\langle E_t^{\text{LCP}} \rangle$  as a function of  $E_t$  observed in ref. [15] is likely due to instrumental distortions. We can account for this saturation by filtering the present measurements of  $^{129}\text{Xe}+^{197}\text{Au}$  with the experimental thresholds present in refs. [14,15]. The resulting distortions to the data are large and induce qualitative changes in the trends of the data, causing an unphysical saturation of  $\langle E_t^{\text{LCP}} \rangle$ . Therefore, the observations listed in [14,15] do not demonstrate any measurable failure of statistical

models that would justify invoking dynamical IMF production by default. While the IMFs may indeed be produced dynamically, the observations listed in refs. [14,15] do not provide evidence for such a conclusion.

### Acknowledgments

This work was supported by the Nuclear Physics Division of the US Department of Energy, under contract DE-AC03-76SF00098, and by the National Science Foundation under Grants No. PHY-8913815, No. PHY-90117077, and No. PHY-9214992. One of us (L.B) acknowledges a fellowship from the National Sciences and Engineering Research Council (NSERC), Canada, and another (A.F.) acknowledges economic support from the Fundación J.B. Sauberaan, Argentina.

### Present addresses:

\* Indiana University Cyclotron Facility, 2401 Milo B. Sampson Ln, Bloomington, IN 47408

† Washington Aerial Measurements Operations, Bechtel Nevada, P.O. Box 380, Suitland, MD 20752

‡ Instituto de Física, Universidade de Sao Paulo, C.P. 66318, CEP 05389-970, Sao Paulo, Brazil

§ Physics Department, Seoul National University, Seoul, 151-742, Korea.

¶ Physics Department, Ohio State University, Columbus, OH 43210

\*\*Dipartimento di Fisica and Istituto Nazionale di Fisica Nucleare, Via A. Valerio 2, 34127 Trieste, Italy

††Physics Department, Hope College, Holland, MI 49423

- 
- [1] D.R. Bowman *et al.*, Phys. Rev. Lett. **67**, 1527 (1991)
  - [2] R.T. Souza *et al.*, Phys. Lett. B **268**, 6 (1991)
  - [3] L.G. Moretto, D.N. Delis, G.J. Wozniak, Phys. Rev. Lett. **71**, 3935 (1993).
  - [4] L.G. Moretto and G.J. Wozniak, Annu. Rev. Nucl. & Part. Sci. **43**, 379 (1993).
  - [5] L.G. Moretto *et al.*, Phys. Rev. Lett. **74**, 1530 (1995).
  - [6] K. Tso *et al.*, Phys. Lett. B **361**, 25 (1995)
  - [7] R. Donangelo, S.R. Souza, Phys. Rev. C **56**, 1504 (1997).
  - [8] L.G. Moretto, R. Ghetti, L. Phair, K. Tso, G.J. Wozniak, Phys. Rep. **287**, 249 (1997).
  - [9] D.H.E. Gross, Phys. Rep. **279** 120 (1997).
  - [10] L. Beaulieu, L. Phair, L.G. Moretto, G.J. Wozniak Phys. Rev. Lett. **81**, 770 (1998).
  - [11] L. Phair *et al.*, Phys. Rev. Lett. **75**, 213 (1995).
  - [12] M. D'Agostino *et al.*, Phys. Lett. B **371**, 175 (1996).
  - [13] L. Phair *et al.*, Phys. Rev. Lett. **77**, 822 (1996).
  - [14] J. Toke *et al.*, Phys. Rev. Lett. **77**, 3514 (1996).
  - [15] J. Toke, D.K. Agnihotri, B. Djerroud, W. Skulski, W.U. Schroeder, Phys. Rev. **C56**, R1683 (1997).
  - [16] R.T. De Souza *et al.*, Nucl. Inst. Meth. **A295**, 109 (1990).
  - [17] Y.D. Kim, R.T. de Souza, D.R. Bowman, N. Carlin, C.K. Gelbke, W.G. Gong, W.G. Lynch, L. Phair, M.B. Tsang,

- and F. Zhu, Phys. Rev. C **45**, 338 (1992).
- [18] W.L. Kehoe *et al.*, Nucl. Inst. Meth. **A311**, 258 (1992).
  - [19] I. Iori *et al.*, Nucl. Inst. Meth. **A325**, 458 (1993).
  - [20] N. Colonna and E. Lisi, Nucl. Inst. Meth. A **334**, 551 (1994).
  - [21] D.R. Bowman *et al.*, Phys. Rev. **C46**, 1834 (1992).
  - [22] D.R. Bowman *et al.*, Phys. Rev. **C52**, 818 (1995).
  - [23] C. Cavata, M. Demoulin, J. Gosset, M.C. Lemaire, D. L'Hote, J. Poitou, O. Valette, Phys. Rev. **C42**, 1760 (1990).
  - [24] L. Phair *et al.*, Nucl. Phys. **A548**, 489 (1992).
  - [25] L. Phair *et al.*, Nucl. Phys. **A564**, 453 (1993).
  - [26] J.P. Bondorf, A.S. Botvina, A.S. Iljinov, I.N. Mishustin, K. Sneppen, Phys. Rep. **257**, 133 (1995).
  - [27] W. Bauer, Phys. Rev. **C38**, 1297 (1988).
  - [28] L. Phair, L. Beaulieu, L.G. Moretto, G.J. Wozniak, Phys. Rev. Lett. **81**, 4021 (1998).
  - [29] D.W. Stracener, D.G. Sarantites, L.G. Sobotka, J. Elson, J.T. Hood, Z. Majka, V. Abenante, A. Chbihi, D.C. Hensley, Nucl. Inst. & Meth. A **294**, 485 (1990).
  - [30] W.J. Llope *et al.*, Phys. Rev. **C51**, 1325 (1995).